DOI:
10.1039/c7sm01893b

Document Version
Peer reviewed version

Journal Name

ARTICLE

Received 00th January 20xx,

Accepted 00th January 20xx

DOI: 10.1039/x0xx00000x

www.rsc.org/

Towards optimised drug delivery: structure and composition of testosterone enanthate in sodium dodecyl sulfate monolayers

Yussif Saaka,[a]† Daniel T. Allen,[b]† Yuvared Luangwitchajaroen,[a] Yanan Shao,[a] Richard A. Campbell,[c] Christian D. Lorenz,[b,]* and M. Jayne Lawrence[a,d]*

Surface tension and specular neutron reflectivity measurements have been used, for the first time to systematically study both the interfacial structure and composition of monolayers of the soluble surfactant, sodium dodecyl sulfate containing a low-dose, poorly water soluble drug, testosterone enanthate. Modelling of the specular neutron reflectivity data suggests that the hydrophobic testosterone enanthate was adsorbed in the C_{12} hydrophobic tail region of the surfactant monolayer, regardless of the concentration of surfactant at the interface and whether or not additional drug was added to the interface. The location of the hydrophobic drug in the tail region of the surfactant monolayer is supported by the results of classical, large-scale molecular dynamics simulations. The thickness of the surfactant monolayer obtained, in the presence and absence of drug, using molecular dynamics simulations was in good agreement with the corresponding values obtained from the specular neutron reflectivity measurements. The stoichiometry of surfactant:drug at the air-water interface at sodium dodecyl sulfate concentrations above the critical micelle concentration was determined from specular neutron reflection to be approximately 3:1, and remained constant after the spreading of further testosterone enanthate at the interface. Significantly, this stoichiometry was the same as that obtained in the micelles from bulk solubilisation studies. Important insights into the preferred location of drug in surfactant monolayers at the air-water interface as well as its effect on the structure of the monolayer have been obtained from our combined use of experimental and simulation techniques.

Introduction

Increasing numbers of therapeutic agents undergoing development as medicines exhibit an extremely poor aqueous solubility. In some classes of therapeutic agent, up to 80-90% of all potential new drug molecules, possess extreme water insolubility.[1-3] This poor water-solubility is a serious limitation when attempting to formulate a drug as a medicine because it frequently results in only a small amount of drug being absorbed from the gastrointestinal tract, i.e. the drug is poorly bioavailable.[1-3] Poor bioavailability renders a drug candidate unsuitable for development into a medicine meaning that the patient will not benefit from the drug. A number of ways have been proposed to increase the apparent aqueous solubility, and thereby the bioavailability, of such drugs including solubilising the drug in surfactant micelles. Unfortunately, the range of commercially available, pharmaceutical acceptable, surfactants is very small, with most having a drug solubilising capacity that is too low to be of practical use. There is therefore an urgent need to design and develop new surfactants with greatly improved drug solubilising capacity for the purposes of medicines development.

Surprisingly little is known, however, about the relationship between surfactant and drug molecular structure and the ability of the micelle to solubilise a drug. Consequently, we have embarked on a study to understand the relationship between a drug and the extent and preferred site of its solubilisation in a surfactant micelle. As the distribution of a drug in a surfactant monolayer is related to its distribution in the corresponding micelles, it is considered that determination of this profile will provide valuable information about the micellar solubilisation of the drug and aid in the design of novel micelles as drug delivery vehicles. When studying drug solubilisation in a surfactant monolayer, two pieces of information are of interest, namely the level of incorporation of drug in the surfactant monolayer, and the location of drug in the monolayer. The only way to unambiguously obtain this information is to use

a. *Institute of Pharmaceutical Sciences. Faculty of Life Sciences and Medicine, King's College London, Franklin-Wilkins Building, Stamford Street, London SE1 9NH, UK.*

b. *Department of Physics, Faculty of Natural and Mathematical Sciences, King's College London, Strand, London WC2R 2LSJ, UK. E-mail chris.lorenz@kcl.ac.uk.*

c. *Institut Laue-Langevin, 71 avenue des Martyrs, BP 156, 38100 Grenoble, France*

d. *Division of Pharmacy and Optometry, School of Health Sciences, Faculty of Biology, Medicine and Health, Stopford Building, University of Manchester, Oxford Road, Manchester, M13 9PT. E-mail jayne.lawrence@manchester.ac.uk.*

specular neutron reflectivity (SNR) in combination with isotopic contrast variation. To our knowledge no research has reported the distribution of a drug in a soluble surfactant monolayer using SNR. Furthermore, while work has been performed using SNR to study the conformation of mixtures at the air-water interface including surfactant, polymer/surfactant and surfactant/protein mixtures (e.g. the comprehensive studies in this area of Penfold, Thomas and Lu), only a very limited amount of work has been carried out on the incorporation into surfactant monolayers of drug-like molecules (e.g. oils[4,5] and perfume-like molecules).[6,7] A key challenge in the current project was data interpretation where small changes in the neutron reflectivity need to be modelled meticulously to reveal physically meaningful information.

Classical, large-scale molecular dynamics (MD) simulations is another method that is commonly used to gain insight into the atomistic interactions that govern the ability of a surfactant to solubilise drug molecules. There have been several studies in which various groups, including ours, have used MD simulations to investigate the solubilisation of various small molecules in surfactant micelles.[8-14] However, very little has been performed using MD simulations to investigate the interaction of drug molecules with soluble surfactant monolayers, and the research that has been undertaken has been focused on drugs interacting with *lipid* monolayers, including thymol with dipalmitoylphosphatidylcholine (DPPC) monolayers,[15] L-phenylalanine with DPPC monolayers,[16] nalidixate calixarene with cholesterol monolayers,[17] and piroxicam with dimyristoylphosphatidylcholine (DMPC) monolayers.[18] To our knowledge, this is the first paper in which molecular dynamics simulations have been used to investigate the interactions between a drug molecule and a soluble surfactant monolayer.

The present study uses a combination of surface tension measurements and SNR with isotopic contrast variation to study the composition (i.e. solubilisation capacity) and structure (location of the drug) of a sodium dodecyl sulfate (SDS) monolayer at the air-water interface for the poorly water-soluble, hydrophobic drug, testosterone enanthate (TE). In this study we have developed, for the first time, an experimental protocol to systematically study the interfacial structure and composition of monolayers containing a low-dose, poorly water soluble drug and a soluble surfactant. Complimentary large-scale molecular dynamic simulations were performed to determine the structure of the SDS monolayers in the absence and presence of TE. We have demonstrated previously the power of combining these experimental and simulation techniques to obtain a detailed description of the interactions between solvents, co-solvents and small molecules with various surfactant and lipidic systems.[11,19,20] The knowledge of the structure and composition of the TE-containing SDS monolayers gained from these studies is an important step in understanding how drug is solubilised in surfactant monolayers and, by implication, surfactant micelles and will lead to the design of new improved surfactants.

Experimental Section

Materials

Protiated sodium dodecyl sulfate (denoted here as h_{25}SDS), testosterone enanthate (TE), D_2O, *n*-hexane, ethanol and chloroform were obtained from Sigma-Aldrich (Poole, UK) and were of the highest grade available. The chemical structures of h_{25}SDS and TE are shown in Figure 1. Tail-deuterated SDS (described as d_{25}SDS) was supplied by the ISIS Oxford Isotope Facility (Didcot, UK). Decon 90 was from Decon Laboratories Limited, (Hove, UK). Ultrapure water, with a resistivity of 18.2 MΩ.cm at 298 ± 0.1 K was from a Milli-Q® Ultrapure Water System (Watford, UK).

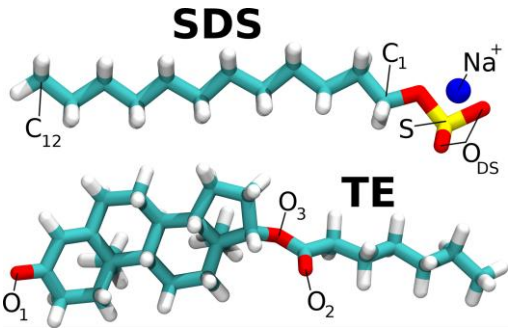

Figure 1: The chemical structures of sodium dodecyl sulfate (SDS) and testosterone enanthate (TE). The colours cyan, grey, red, yellow and blue represent the elements, carbon, hydrogen, oxygen, sulfur and sodium, respectively.

Experimental protocols

The surface tension of SDS solutions of 0.1, 0.2, 0.5, 1.0, 1.5 and 2.0 times the critical micelle concentration (CMC) was first measured in the absence of TE. (Note that the CMC of the SDS used in the study was confirmed to be 0.23 w/v, as previously determined.[21]) In preliminary surface tension measurements, TE dissolved in *n*-hexane was carefully added (using a Hamilton syringe) to the surface of aqueous SDS solutions of differing concentrations. However, a considerable amount of TE could be added both above and below the CMC before any noticeable effect on surface tension was observed. This effect was attributed to dissolution of TE in the aqueous sub-phase at SDS concentrations below the CMC (a TE aqueous solubility of 0.00017 % w/w[22,23] has been reported) while, in addition, above the CMC solubilisation of TE in surfactant micelles (see the Supplementary Information, Figure SI1). Therefore, we developed a two-part protocol to ensure that we were measuring mixed monolayers of surfactant and drug at equilibrium. It should be noted further that preliminary surface tension experiments indicated that the presence of a saturation amount of TE did not significantly change the CMC of SDS (see Results and Discussion).

In the first part of the protocol, the effect of TE on the surface tension of SDS was determined at the same surfactant concentrations listed above. To determine the influence of a saturation amount of TE on the surface tension of micellar SDS solutions (i.e. 1.0, 1.5 and 2.0 times the CMC), an excess amount of TE was added to each of the surfactant solutions and incubated for at least 6 hours (the time previously determined to be necessary for equilibration), before the excess TE was removed by filtration

through a 0.22 µm cellulose acetate filter (Millipore. Watford, UK). Preparation of the TE-saturated micellar SDS solutions in this way ensured that both the aqueous continuous phase and any micelles present were saturated with TE. When establishing the effect of TE-saturation on SDS solutions at concentrations less than the CMC (i.e. 0.1, 0.2 and 0.5 times the CMC), it was sufficient simply to prepare the solutions using TE-saturated water. In addition, to validate this approach, a sample containing SDS below its CMC (i.e. 0.1 times the CMC) was also made in the same way as the SDS solutions above their CMC. The surface tension of the solutions thus prepared was measured as described below and was observed to be the same as the corresponding SDS solution prepared using TE saturated water. Conversely, however, the surface tension of an SDS solution at the CMC was higher (i.e. c.f. to that of the equivalent SDS solution) when prepared using TE saturated water than when the SDS solution was saturated with TE, suggesting that there was insufficient TE to saturate the micelles at the CMC in the former case. It is worth noting that the surface tension of TE-saturated water was 71.3 ± 0.5 mN m^{-1}, i.e. not significantly different from that of TE-free water.

The second part of the protocol was performed to confirm that the material at the air-water interface was saturated with an equilibrium amount of TE. To achieve this, 10 µL of a 5.2×10^{-1} mg mL^{-1} solution of TE dissolved in *n*-hexane was carefully spread on the surface of the TE-saturated SDS solutions in a drop wise manner using a Hamilton syringe and the surface tension of the surfactant solutions re-measured after sufficient time had been left for the *n*-hexane to evaporate, typically 10 minutes. Preliminary surface tension experiments demonstrated that the addition of n-hexane alone to the surface of water and to the surface of SDS solutions in the absence of TE did not alter the surface tension, supporting the hypothesis that the n-hexane rapidly evaporated under the conditions of study. The amount of TE in *n*-hexane added to the surface of the SDS solution to ensure saturation was calculated by determining the number of SDS molecules required to form a complete monolayer on the surface of a Teflon™ trough of dimensions of 5.7 cm × 15.5 cm (i.e. the trough used for surface tension measurement), and assuming an area per SDS molecule, at the CMC, of 44 ± 4 $Å^2$ (Lu et al.[24]) and then multiplying this number by the molar ratio of SDS:TE in the surfactant micelle at saturation, namely, 3.2:1.[21]

SNR experiments were performed using the same protocols as described above for surface tension measurements. Note that the value of the CMC of 0.23 % w/v obtained from surface tension measurements of h_{25}SDS on ultrapure H_2O, was used in the SNR studies, after correction for the difference in molecular weight when using deuterated surfactant.

Terminology

The monolayers examined in the present study by surface tension and SNR are described according to their preparation method. For example, sample 1.0s denotes that the SDS solution at the CMC had been saturated with TE while sample 1.0s+TE denotes the spreading (from *n*-hexane) of additional TE onto the surface of the TE-saturated SDS solution. The same notation is used for SDS solutions at concentrations greater than their CMC. For SDS monolayers at concentrations below the CMC, 0.5s indicates that the SDS solution at 0.5 times the CMC was prepared in TE-saturated water while 0.5s+TE denotes the spreading of additional TE onto the surface of sample 0.5s. The presence of `o' represents TE-free (i.e. SDS only) solutions at the concentration indicated.

Surface tensiometry

The surface tension of aqueous solutions of SDS in the presence and absence of a saturation amount of TE at 298 ± 0.1 K was measured using a K11 Tensiometer (KRÜSS GmbH, Villebon sir Yvette, France) and the non-detachment Wilhelmy plate method to allow any changes in surface tension with time to be monitored. The Wilhelmy plate used in the study was made from platinum and prior to its use was cleaned by passing through a naked bunsen flame. The surfactant solutions were contained in a Teflon™ trough of dimensions of 5.7 cm × 15.5 cm for measurement. Prior to use, the trough was washed first with Decon 90 detergent, then pure water, then ethanol and chloroform. In addition, precautions were taken to ensure that any glassware with which the surfactant solutions came into contact was scrupulously cleaned namely, first by soaking overnight in Decon 90 and then extensively rinsing, first with tap water and finally with ultrapure water. The surface tension of each surfactant solution was measured in triplicate using three individually prepared samples, with the surface tensions quoted being that recorded when the system under study had reached equilibrium - assessed by no change in surface tension upon repeated measurement, occurring in all cases within 10 minutes. The external accuracy of the measurements was checked by the frequent measurement of the surface tension of ultrapure water, a value within the range 72.0 ± 0.4 mN m^{-1} at 298 ± 0.1 K was considered acceptable.[25]

SNR experiments

SNR measurements on SDS monolayers in the presence and absence of saturation amounts of TE were performed on the Fluid Interfaces Grazing Angles ReflectOmeter (FIGARO) at the Institut Laue-Langevin (Grenoble, France).[26] A pair of choppers was used to give pulses of neutron wavelengths in the wavelength range 2-30 Å at a resolution in momentum transfer of 8 %. The SNR data were recorded on samples contained in Teflon™ troughs (dimensions 22 cm x 5 cm), and were collected at fixed neutron incidence angles of 0.62^o and 3.8^o. The neutron reflectivity profiles presented are the intensity ratio of the neutrons in the specular reflection to those neutrons in the incident beam, corrected for background scattering, as a function of the momentum transfer, Q_z, defined by:

$$Q_z = 4\pi.\sin\theta/\lambda \quad (1)$$

where θ is the angle of incidence, and λ is the wavelength. The principle of the application of this technique at the air-water interface has been described elsewhere,[27] and a recent review article has summarised the application of SNR to the study of various systems at fluid interfaces.[28]

In all cases the troughs used for the measurements were placed on a six-compartment sample changer and were individually sealed. A laser was employed in the automatic height alignment of the samples. 5-minute time slices of the SNR were collected repeatedly, to ensure that the samples had equilibrated before the

data were summed to optimise the signal/noise ratio. In all cases the samples were found to have equilibrated by the time the first 5-minute time slice was recorded. In a limited number of cases, samples were observed using SNR for up to 24 hours to confirm equilibration had been reached; in no instance was any change to the SNR recorded.

The mixed SDS/TE solutions were prepared in four different isotopic contrasts: two contrasts of solvent, D_2O (scattering length density (SLD) = 6.36×10^{-6} Å^{-2}) and air contrast-matched water, ACMW (a mixture of 8.1 % by volume D_2O in H_2O with a scattering length density of 0 Å^{-2}), and two different isotopic contrasts of surfactant, h_{25}SDS and d_{25}SDS.

SNR modelling approach

The experimental neutron reflectivity profiles were modelled by fitting to calculated SLD profiles with respect to the isotopic contrast in the direction normal to the surface. The calculated SLD profiles were obtained by assuming that the surface structure consisted of a number of stratified layers parallel to the interface. Each layer was defined by its SLD (ρ), thickness (d) and roughness (σ), and these quantities were either refined or constrained to physically realistic values in order to obtain the best fit to the experimental data. The SLDs used were calculated using the scattering lengths and molecular volumes of the respective chemical species as shown in Table 1. In brief, the modelled SLD profiles in different contrasts were co-refined to fit the experimental data using the program, Motofit.[29]

Table 1: The molecular formula, molecular volume, molecular weight, mass density, scattering length and scattering length density of protiated testosterone enanthate and protiated and deuterated sodium dodecyl sulfate.

Material	Molecular formula M_f	Molecular volume V_m (Å^3)	Molecular weight M_{wt} (g mol)	Mass density 〉 (g mL^{-1})	Scattering length (10^{-5} Å)	Scattering length density (10^{-6} Å^{-2})
h_{25}SDS	$NaC_{12}H_{25}SO_4$	414.4	288.38	1.16	15.93	0.39
d_{25}SDS	$NaC_{12}D_{25}SO_4$	414.4	313.03	1.25	276.22	6.66
SS	$NaSO_4$	60.7	119.05	3.25	29.69	4.89
h_{25}	$C_{12}H_{25}$	353.7	169.33	0.79	-13.76	-0.39
d_{25}	$C_{12}D_{25}$	353.7	194.48	0.91	246.53	6.95
TE	$C_{26}H_{40}O_3$	630.6*	400.59	1.05	40.58	0.64

*Calculated ab initio[29]
SS denotes the SDS head group and counterion

SNR structural analysis

Five different structural models of stratified layers normal to the air-water interface were used to evaluate the location of TE in SDS monolayers for the sample of 2.0 CMC SDS with additionally spread TE (2.0s+TE) measured in all 4 isotopic contrasts. In Models 1 and 2, the SDS layer was approximated to a single combined layer of tails and head groups (including counterions). Model 1 comprised a single uniform layer of SDS, TE and solvent whilst Model 2 comprised a single uniform layer of SDS, below which there was a second uniform layer of TE and solvent. In Models 3, 4 and 5, the SDS layer was approximated to be divided into one uniform layer comprising of tails (in contact with the air) below which was another layer of head groups and solvent. For Model 3, TE was located in layer 1 (i.e. the tail region), for Model 4 it was located in layer 2 (i.e. the head group region), and for Model 5 it was located in a third layer beneath the other two.

The roughness of all layers was fixed at 4.0 Å in accordance with the results obtained from capillary-wave experiments for surfactant solutions.[30,31] The thickness of the SDS head group was systematically varied from 2 to 5 Å in 0.5 Å increments to find the optimum value. A value of 4.0 Å for the head group thickness was found to give the best model fitting results and is consistent with its physical size. The tail group volume fraction in Models 3, 4 and 5 was assumed to be 1 because the surfactant tails are in a fluid phase. A simultaneous fit was performed on data recorded in all 4 contrasts. A detailed description of the fitting procedure for all models used in this study is given in the Supplementary Information.

SNR compositional analysis

It is described in the Results and Discussion section that Model 3 gives the best fitting results for the location of the drug in the surfactant monolayer, so it was applied in the compositional analysis. Due to extremely small changes in the experimental data resulting from the incorporation of TE in the monolayer for the data of the 2 isotopic contrasts involving h_{25}SDS in relation to the small but finite systematic errors in the data, the precision in our ability to resolve the interfacial composition was in fact reduced from their inclusion in the analysis (i.e. the fits were worse in the regions where the surface excesses of the components had a marked effect on the data), so they were omitted. The surface excesses of surfactant and TE were determined by fitting different regions of the data in 2 isotopic contrasts involving d_{25}SDS that were sensitive to the parameters of interest using the 'fit with cursors' option of the fitting software, rather than a global fit of the full *Q*-range where sub-percent systematic errors in the data combined with extremely low error bars in different *Q*-ranges in fact reduced the precision by which we were able to resolve the interfacial composition. The surface excesses of both SDS and TE were obtained from the data of TE with d_{25}SDS on ACMW at low *Q* and the data of TE with d_{25}SDS on D_2O at high *Q*, respectively. The surface excess of SDS was adjusted until the fitting the model to the experimental data in the range *Q* range 0.05–0.10 Å^{-1} for d_{25}SDS on ACMW. The surface excess of TE was then adjusted in the range *Q* range 0.10–0.15 Å^{-1} for d_{25}SDS on D_2O. These two steps were then performed iteratively until the best fit of the model to the data was achieved. This procedure resulted in the least scatter

in the resulting interfacial compositions with respect to the bulk composition. While this procedure may be considered unconventional, it was necessitated by the challenge to quantify extremely small changes in the experimental data with a total interfacial thickness of less than 20 Å and weakly scattering drug molecules to give physically meaningful results.

The reason why we could not use the low-Q compositional analysis method developed recently on FIGARO[32] where the interfacial composition is solved accurately by fast measurements only at low Q in the two isotopic contrasts involving ACMW, was because of the low SLD of the drug in the present study.

Description of simulations

Results are reported from five all-atom molecular dynamics (MD) simulations which were performed to emulate some of the experimental systems from which results are reported in the current study. These simulations investigate how varying both the number of TE molecules and the area per surfactant affects the structure of SDS monolayers at the air-water interface. For the most part, the area per surfactant molecule (in units of $Å^2$) used for the simulation was that determined experimentally from the analysis of the SNR data at the relevant SDS concentration. The naming scheme for the simulations aligns to that used for the experimental studies in that: MD0.1o represents a TE-free SDS monolayer simulated at an area per surfactant molecule corresponding to that experimentally determined for an SDS solution 0.1 times the CMC. Similarly, MD0.1s denotes a simulated SDS monolayer prepared at a SDS concentration 0.1 times the CMC using TE saturated water (here 1 TE molecule was added to each SDS monolayer to mimic this condition), while MD0.1s+TE represents the corresponding system in which an excess of TE has been added to the surface, in this case 32 molecules of TE were present in each SDS monolayer. Finally, two simulations representing SDS monolayers at or above the CMC were studied. One system denoted MD1.0s+TE, represented a system in which the SDS micellar solution was saturated with TE and to which additional TE in hexane was added to the surface of the monolayer, while MD1.0ss+TE+TE was similar but with an additional (second) aliquot of TE in hexane added to the monolayer surface, resulting in a SDS monolayer which has been oversaturated with TE. The SDS to TE ratio for each of the simulated systems is reported below.

All simulations were built and conducted in the same manner, as described briefly below. First the initial structures of the monolayers were built using the Packmol software package.[33] Each system consists of two surfactant monolayer leaflets separated by a 60 Å thick water slab such that the density of water is equal to 1 g mL^{-1}. The number of SDS monomers present per leaflet and the cross-sectional area in the *x*-*y* plane of the simulation box were chosen such that a desired area per surfactant was achieved. The systems were then neutralised by the addition of an appropriate number of Na^+ counterions per leaflet, which were initially placed near the head group regions of the SDS molecules. TE molecules (where appropriate) were then placed in the vacuum region above the top monolayer and below the bottom one (see Figure 2). The placement of the TE molecules in these regions was performed to mimic the placement of the drug in the experiments in which *n*-hexane is used to deliver the drugs onto the hydrocarbon tails of the surfactant monolayers. The *z*-dimension of the simulation boxes were set to 200 Å in all simulations to ensure that there was a sufficiently large vacuum region which eliminates interaction between monolayers through the periodic boundaries in the *z*-dimension.

Once the initial structures had been built, energy minimisation runs were conducted using 100,000 as the maximum number of force/energy evaluations. The minimised states of the systems were then simulated in the constant NVT ensemble for 10 ns to achieve thermalisation. Finally, 50 ns production runs were performed using the NVT ensemble, which were analysed to produce the results presented below.

All monolayer simulations were performed using the LAMMPS simulation package[34] with the CHARMM force field[35,36] for the description of both inter and intra-molecular interactions of the SDS[37,38] and TE.[35] The TIP3P water model[39] was used to describe interactions involving water. The van der Waals interactions were cut-off at 10 Å whilst the electrostatic interactions were cut-off at 12 Å. The PPPM method[40] was used to compute long-range Coulombic interactions. The equilibration and production runs for all monolayer simulations utilised the Nose-Hoover thermostat[41] to fix the system temperature at T = 300 K. A time step of 2 fs was used in all simulations to ensure stable integration of Newton's equations of motion with the velocity Verlet algorithm whilst all hydrogen-containing bonds and the valence angle of water molecules were constrained using the SHAKE algorithm.[42] The centre of mass of the systems was constrained to be at the centre of the box, *z* = 0, throughout the simulations to enable easy visualisation and analysis. The measurements discussed in the following sections were conducted using the entirety of the production periods obtained for each simulation.

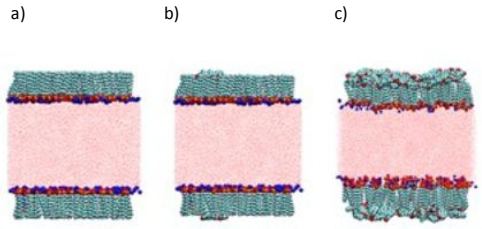

Figure 2: Initial configurations of three of the SDS monolayer simulations with or without TE: a) MD0.1o, b) MD0.1s and c) MD0.1s+TE where MD indicated a monolayer simulation, 0.1 is 0.1 x CMC of SDS, 0.1o denotes the absence of TE from the SDS solution, MD0.1s represents the SDS solution prepared using TE saturated water while sample MD0.1s+TE approximates the spreading of additional TE onto the surface of the TE-saturated SDS solution. The water is represented as points to clearly see the other components of the system. In all figures, the colours cyan, grey, red, yellow and blue are used to represent the elements: carbon, hydrogen, oxygen, sulfur and sodium respectively.

Analysis of MD trajectories

To characterise the SDS monolayer structure, the various measures of the structural properties depicted in Figure 3 have been

performed using the MD trajectories and the effects of area per surfactant molecule and the ratio of SDS to TE have been investigated. The instantaneous thickness of the head group region of the SDS monolayer, *d*-head, is defined as the magnitude of the vector from the surfactant oxygen atoms within the same surfactant molecule which are closest and furthest away from the centre of the simulation box when projected onto the z-axis and then averaged over all surfactant molecules. The chain thickness, *d*-tail, is defined as the magnitude of the vector pointing from C1 to C12 atoms within the same surfactant molecule, when projected onto the z-axis and then averaged over all surfactant molecules. *d*-tail measurements exhibit small fluctuations around mean values for the entirety of the last 10 ns in all of the simulations which suggests that all monolayers are well equilibrated during this time.

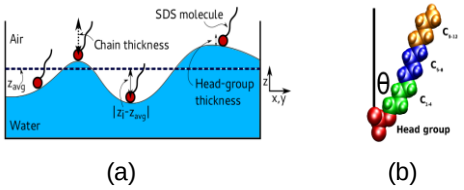

Figure 3: (a) A schematic diagram of the different structural properties of SDS monolayers which are reported in the manuscript. The average *z*-coordinate of the SDS head groups in a monolayer is depicted by the thick dashed line. From this, monolayer roughness (exaggerated in the schematic for clarity) is quantified by calculating $|z_i\text{-}z_{avg}|$. The chain thickness, *d*-tail and head group thickness, *d*-head, measurements are also shown. **(b)** A diagram which illustrates how the position of the TE in the SDS monolayer is determined as a function of the mean tilt angle of the hydrocarbon tail, ϑ_t.

As the majority of the quantities of interest in these simulations are measured in relation to their distance from the interface of the SDS monolayers, it is important that the location of this interface is unambiguously defined. Therefore, in this manuscript, the definition of the interface between the SDS monolayers and the aqueous phase is described using an *intrinsic surface,* which is determined using the algorithm proposed by Sagar *et al.*[43] In essence, this method is performed by projecting the location of a particle of interest and the anchor points, which in these systems are the sulfur atoms in the SDS head group, used to define the interface onto the *x*-*y* plane. Next, the closest anchor point to the particle of interest within this projected two-dimensional representation is established. Finally, the location of the intrinsic surface for the particle of interest is assigned the value of the *z*-coordinate of the closest anchor point (see the Supplementary Information, Figure SI2).

The intrinsic density is used to describe the average density of different atomic species as a function of their distance away from the intrinsic surface and is defined mathematically as:

$$\bar{\rho}(z) = \left\langle \frac{1}{A_0} \sum_{i=1}^{N} \delta(z - z_i + \xi(\boldsymbol{R}_i)) \right\rangle \quad (1)$$

where the summation indexed by *i* runs over all *N* particles of a given atomic species, $\xi(\boldsymbol{R}_i)$ represents the *intrinsic surface* for a given configuration, $\boldsymbol{R}_i=(x_i,y_i)$ is the location of particle *i* in the *x*-*y* plane for a given configuration and A_0 is the cross sectional area of the interface. The *z*-coordinate of the i^{th} particle is denoted by z_i and *z* represents the vertical distance from the SDS/water interface to particle *i* where values of $z > 0$ and $z < 0$ represent locations within the water slab and towards the vacuum region, respectively.

The structure of the monolayer can also be considered in terms of angles formed between different parts of the surfactant molecules and a unit-vector in the z-direction. The surfactant chain tilt angle, ϑ_t, is defined as the angle between the vectors formed between the C1 atom (the head group carbon) and the C12 atom (the carbon of the terminal methyl group) and a unit vector in the *z*-direction. When this angle is zero, the hydrocarbon tail is perfectly aligned with the *z*-axis and when this angle is 90°, the SDS molecule is lying in the *x*-*y* plane. The SDS head group tilt angle, ϑ_h, was also measured for all of the monolayer systems and is defined as the angle between the vector formed between S (the sulfur atom in the SDS head group) and C1 atoms, and the vector formed between C1 and C12 atoms. When this angle is zero, the entire molecule is aligned linearly and when this angle is 90° the head group is oriented such that it is perpendicular to the SDS hydrocarbon chain.

The orientation of a TE molecule is described by the cosine of the angle formed between the vector pointing from the O1 atom to the O2 atom (Figure 3) in TE and a unit vector: (0,0,1) or (0,0,-1) for TE molecules in the top or bottom monolayer leaflets respectively. When $\cos(\vartheta)$ is equal to -1, the entire TE molecule is aligned parallel to the *z*- axis with the O2 atom pointing towards the vacuum region and the O1 atom pointing towards the water slab, when $\cos(\vartheta)$ is equal to 0 the TE molecule is oriented in the *x*-*y* plane and when $\cos(\vartheta)$ is equal to 1, the TE molecule is again aligned parallel to the *z*-axis but with the O1 atom pointing towards the vacuum region and the O2 atom pointing towards the water slab. The location of a TE molecule is defined as the midpoint of the vector connecting the O1 and O2 atoms. In this case, the angle distributions are calculated as a function of the distance from the intrinsic surface of the SDS monolayer into the hydrocarbon tail region. For clarity, four distinct regions are defined, namely the head group, C1-4, C5-8 and C9-12. The size of these regions vary as a function of the mean surfactant chain tilt angle as shown in Figure 3(b). The region boundaries for a given TE molecule are obtained from the *z*-coordinates of the relevant carbons on the nearest SDS molecule.

The effect that the presence of TE has on the hydration of the SDS head groups was investigated by calculating the radial distribution functions, g(r), between the sulfur atom in the SDS

head group and the hydrogen and oxygen atoms in the neighbouring water molecules. Using the nearest neighbour distances, taken to be the distance corresponding to the first minimum in the g(r) curve, it was possible to determine the number of water of hydration molecules around a given atom in a molecule by averaging the number of water molecules that are within the nearest neighbor distance in g(r), while taking precautions not to double count any water molecule.

Results and discussion

Surface Tensiometry

Figure 4 shows the effect of the presence of a saturation concentration of TE on the surface tension of an aqueous SDS solution at SDS concentrations ranging between 0.1 to 2 times the CMC as well as the effect of the addition of extra TE (added to the surface in the form of a *n*-hexane solution) on the value of the equilibrium surface tension.

The surface tension values of SDS solutions below the CMC with and without TE are equivalent, which suggests the presence of a rather low amount of TE at the air-water interface. Nevertheless, in the interpretation of these data we must recall that the surface tension is not a direct measure of the surface excess of either component but instead a measure of the lowering of free energy of the interface as a result of the interactions of both components. For additional insight into the relative and absolute amounts of each component at the interface, SNR is required, as demonstrated below. For the TE-containing micellar SDS solutions, the measured surface tension is clearly lower than that obtained for TE-free micellar SDS solutions. This observation demonstrates that the presence of TE in the SDS monolayer reduces surface tension. In this context, it is of note that the surface tension of TE-saturated water was 71.3 ± 0.5 mN m^{-1}, i.e. not significantly different from that of TE-free water.

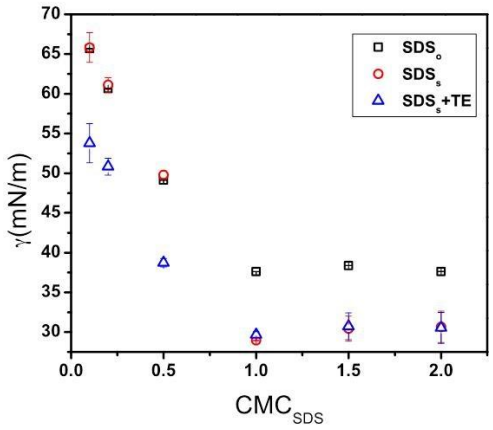

Figure 4: Variation in surface tension with SDS concentration expressed as a function of the bulk surfactant concentration with respect to its critical micelle concentration (CMC_{SDS}) at the air-water interface at temperature, T = 298 ± 0.1 K for TE-free SDS (SDSo), SDS in the presence of saturation amounts of TE (SDSs), and with additional TE spread on the surface of SDS in the presence of saturation amounts of TE (SDSs+TE).

For micellar SDS solutions, there is little/no change in surface tension following the spreading of additional TE in *n*-hexane onto the air-water surface of the TE-saturated SDS solutions, supporting the hypothesis that the surface is already saturated with TE and that the additional spreading TE does not significantly affect the composition of the TE-saturated SDS monolayer. This observation contrasts with the corresponding results at SDS concentrations below the CMC where there is a clear reduction in surface tension upon the spreading of additional TE in *n*-hexane suggesting that under these conditions there is a significant change in the monolayer composition, most likely by the insertion of more TE into the surfactant monolayer. These observations are explored in more detail using SNR and molecular dynamics simulations below.

Specular Neutron Reflectometry

Structure of sodium dodecyl sulfate monolayers in the presence of testosterone enanthate

The specular neutron reflectivity profiles for all four isotopic contrasts of TE-saturated SDS solutions at 2 times the CMC, after the additional spreading of TE at the interface (i.e. 2.0s+TE according to our terminology), together with the best fits obtained using each of the five models employed to divide regions of molecules (or parts of molecules) normal to the

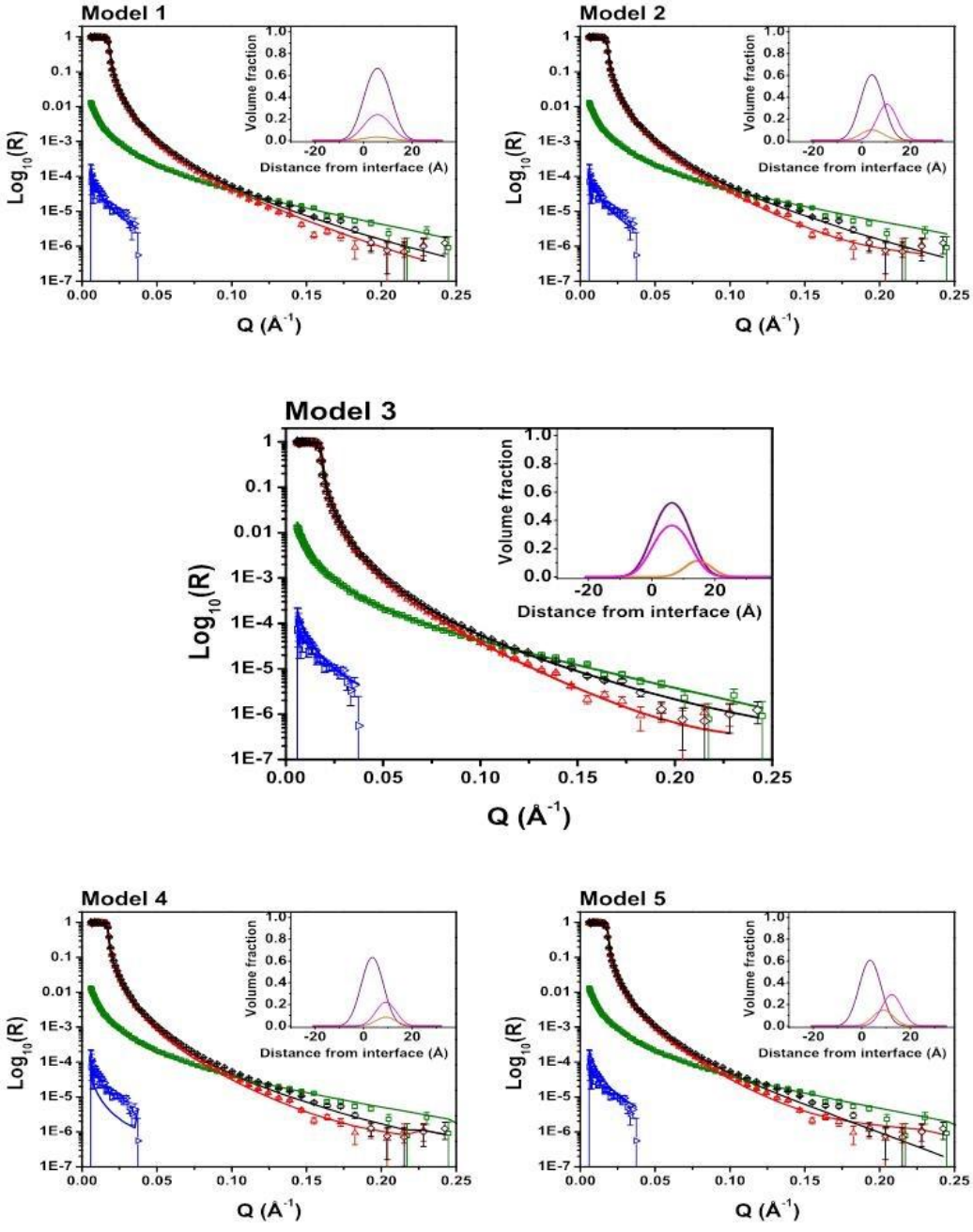

Figure 5: Specular neutron reflectivity profiles for the adsorption of SDS and TE at the air-water interface after the additional spreading of TE in a carrier solvent at temperature, T = 298 ± 0.1 K, where the data represent TE with d_{25}SDS in ACMW (green), d_{25}SDS in D_2O (red), h_{25}SDS in ACMW (blue) and h_{25}SDS in D_2O (black). The solid lines represent the calculated simultaneous model fits using the global fit routine. Insets represent volume fraction profiles as a

function of distance to the interface, where the components are SDS tails (purple), SDS head groups including counterions (orange) and TE (pink).

interface are shown in Figure 5. These models are described in the experimental section and for convenience are summarised in Table 2. Also shown in Figure 5 as inserts, are the volume fraction profiles of the SDS tails, SDS head groups (including counterions) and TE as a function of distance to the interface. All the other experimental specular neutron reflectivity profiles obtained in this study, together with their best model fits, are included in the Supplementary Information, Figures SI3 and SI4.

Table 2: Summary of the structural models used in this study to analyse the SNR data.

	Composition of the Layer				
Layer	**Model 1**	**Model 2**	**Model 3**	**Model 4**	**Model 5**
1	SDS & TE	SDS	SDS_{tail} & TE	SDS_{tail}	SDS_{tail}
2	N/A	TE	SDS_{head}	SDS_{head} & TE	SDS_{head}
3	N/A	N/A	N/A	N/A	TE

SDS_{tail} = SDS tails

SDS_{head} = SDS head groups

N/A = not applicable

Although the observed deviations of the fits to the experimental data in the various models are small, they are statistically significant. We infer that Model 3, with TE adsorbed in the C_{12} tail region of the monolayer, and a separate hydrated head group region beneath, produces the best model fitting results. This observation was evident in all the systems and contrasts used in the present study. The reasons for this interpretation are as follows. Model 1 fails to resolve the structure of the SDS/TE monolayer because the fitting model for the d_{25}SDS in D_2O contrast is above the data. The fitting model obtained from Model 2 is worst as it is above the data for the d_{25}SDS in ACMW contrast, and below the data for the h_{25}SDS in D_2O contrast. Model 4 fails to fit the data for the h_{25}SDS in ACMW contrast while Model 5 inadequately fits the data for the h_{25}SDS in D_2O and d_{25}SDS in D_2O contrasts.

It is interesting to note that the results obtained from Model 3, which best describes the data in Figure 5, are consistent with results obtained from small-angle neutron scattering studies which suggest that TE is solubilised in the tail region (i.e. the hydrophobic core) of the SDS micelles.[21] Further, these findings are confirmed below using molecular dynamics simulations.

Information that can be extracted from the application of Model 3 to the SNR data includes the observation that the volume fraction of water in the SDS head group region, VF_{H2O}, remains approximately the same, within experimental error, in the SDS/TE monolayers above and below the CMC before the additional spreading of TE at the air-water interface, as shown in Table 3a. Furthermore, the area per SDS molecule, a_1^s, is consistent at micellar SDS concentrations whereas an increase in a_1^s is observed as the SDS concentration decreases below the CMC. TE dissolved in *n*-hexane was spread on the SDS monolayer with a view to ensuring saturation adsorption of TE at the interface subsequent to the

Table 3: Fitting parameters obtained from the co-refined modelling of the specular neutron reflectivity profiles of SDS/TE monolayers at the air-water interface at temperature, T = 298 ± 0.1 K (a) before and (b) after the additional spreading of TE.

(a) Interfacial properties of SDS/TE monolayers before spreading of additional TE

CMC^*_{SDS}	d_{tail} (± 1 Å)	VF_{H2O} (± 5%)	$\wp_{SDS}$ (10^{-10} mol cm^{-2})	a^s_1 (± 2 $Å^2$)	$\wp_{TE}$ (10^{-10} mol cm^{-2})	Composition (SDS:TE)
0.1_s	7.0	65	2.38	70	0.50	5:1
0.2_s	9.0	66	3.08	54	0.64	5:1
0.5_s	11.1	65	3.82	44	0.77	5:1
1.0_s	12.5	60	3.72	45	1.18	3:1
1.5_s	13.9	70	3.95	42	1.42	3:1
2.0_s	12.6	70	3.52	47	1.32	3:1

(b) Interfacial properties of SDS/TE monolayers after the spreading of additional TE

CMC^*_{SDS}	d_{tail} (± 1 Å)	VF_{H2O} (± 5%)	$\wp_{SDS}$ (10^{-10} mol cm^{-2})	a^s_1 (± 2 $Å^2$)	$\wp_{TE}$ (10^{-10} mol cm^{-2})	Composition (SDS:TE)
0.1_s + TE	8.4	84	1.33	125	1.45	1:1
0.2_s + TE	11.2	75	2.02	82	1.80	1:1
0.5_s + TE	9.0	80	1.75	95	1.38	1:1
1.0_s + TE	11.4	55	2.99	56	1.31	2:1
1.5_s + TE	12.7	65	3.58	46	1.31	3:1
2.0_s + TE	12.7	64	3.50	48	1.37	3:1

CMC* represents a product of the CMC (i.e. 0.23% w/v)[21]

Head group thickness (d_{head}) = 4.0 Å

Roughness of all layers = 4.0 Å

1.0_s + TE and 1.5_s + TE were modelled using data in 2 and 3 contrasts, respectively.

vapourisation of *n*-hexane. Upon the injection of interfacial-saturation amounts of TE at the interface, d_{tail} remained approximately the same at micellar concentrations of SDS whilst d_{tail} varied below the CMC. Similarly, a_1^s and VF_{H2O} are unchanged for 1.5s+TE and 2.0s+TE, and slightly higher for 1.0s+TE. This observation further supports the achievement of equilibrium in the systems at micellar SDS concentrations.

In contrast, the fitting results reveal a drastic increase in a_1^s upon the spreading of additional TE below the CMC. After the additional spreading of TE below the CMC, there is a decrease in $\wp_{SDS}$ and an increase in $\wp_{TE}$ with an expected increase in VF_{H2O} from approximately 65 % to 80 %. These results demonstrate a change in monolayer composition, and the achievement of a new adsorption equilibrium after the additional spreading of TE at the air-water interface.

Composition of sodium dodecyl sulfate monolayers in the presence of testosterone enanthate

Model 3 was used to evaluate the composition of SDS and TE in the monolayer of samples with 6 different bulk surfactant concentrations, as it yielded the best fit to the SNR data in the structural analysis above; data in only 2 isotopic contrasts were used to resolve most precisely the interfacial composition as explained in the Experimental Section.

Prior to the additional spreading of TE, there is no noticeable change in surface excess of SDS, $\wp_{SDS}$ and surface excess of TE, $\wp_{TE}$ with respect to micellar SDS solutions, as is shown in Figure 6 and Table 3. The stoichiometry of SDS:TE remains unchanged at ~ 3:1 for concentrations of SDS above the CMC, indicating maximum adsorption of SDS and TE at the air-water interface. In contrast, $\wp_{SDS}$ and $\wp_{TE}$ increase with SDS at concentrations below the CMC from 2.4×10^{-10} mol cm^{-2} to 3.8×10^{-10} mol cm^{-2} for SDS at concentrations of 0.1 and 0.5 times the CMC, respectively. Additionally, the stoichiometry of SDS:TE remains at approximately 5:1 for SDS at concentrations of 0.1 to 0.5 times the CMC. While the increase in $\wp_{SDS}$ and $\wp_{TE}$ for SDS concentrations ranging from 0.1 to 0.5 times the CMC suggest sub-maximal adsorption of SDS and TE at the air-water interface, the stoichiometry suggests the achievement of equilibrium.

After the additional spreading of TE, a decrease in the average $\wp_{SDS}$ from 3.1×10^{-10} mol cm^{-2} to 1.7×10^{-10} mol cm^{-2} is evident at SDS concentrations below the CMC. On the other hand, the average $\wp_{TE}$ increases from approximately 0.64×10^{-10} mol cm^{-2} to 1.54×10^{-10} mol cm^{-2}. At SDS concentrations below the CMC, the ratio of SDS:TE decreases from the 5:1 stoichiometry observed prior to spreading additional TE to a 1:1 stoichiometry. The decrease in $\wp_{SDS}$ with a corresponding increase in Γ_{TE} after the additional spreading of TE suggests a competitive interaction between SDS and TE at the air-water interface. Whilst a change was observed in $\wp_{SDS}$ and $\wp_{TE}$ below the CMC in the presence of additional TE, the surface excess remains approximately at the same level at micellar concentrations of SDS.

In contrast to the results obtained for SDS/TE monolayers below the CMC, the stoichiometry for SDS:TE at surfactant concentrations of 1.0, 1.5 and 2.0 times the CMC remains at 3:1 after spreading of additional TE at the interface. However, Γ_{SDS} at the CMC is slightly lower after the additional spreading of TE at the interface although stoichiometry results suggest equilibrium conditions. This observation reflects the surface-tension minimum observed at the CMC. The consistent surface excess and stoichiometry determined from the SNR measurements for the SDS/TE monolayers above the CMC, in the concentration range studied, is evidence of saturation of the bulk and interface of the micelle solutions with SDS and TE prior to the additional spreading of TE. It can be inferred from the composition studies at micellar concentrations of SDS that the stoichiometry observed at the interface reflects that observed in micelle solubilisation studies.[21]

It is evident from the composition studies that SDS/TE mixtures at micellar concentrations of SDS are in equilibrium prior to the additional spreading of excess TE at the interface. The consistent composition of SDS:TE at SDS concentrations below the CMC before the spreading of TE at the interface similarly suggests the achievement of equilibrium in these systems. After the additional spreading of TE at the interface of SDS solutions below the CMC, a change in the composition of the monolayer was observed from a constant composition of 5:1 to an equimolar amount of SDS to TE, indicating a perturbation of the equilibrium in the original samples. Furthermore, although the total surface excess of the SDS/TE monolayers remained constant at about 3.5-4.0 10^{-10} mol cm^{-2}, the number of molecules of SDS at the surface decreased by about 45-65%, being replaced with TE molecules which increased their number by a similar extent. It is perhaps not surprising that the TE remains at the interface because under these conditions the aqueous solution is already saturated with TE, while in contrast, because of the ability of SDS to form micelles the aqueous phase can accommodate more surfactant. From a drug delivery standpoint, the use of the least amount of surfactant to achieve the best level of drug loading is essential. Therefore, based on the composition studies, the best concentration range of SDS to achieve the most efficient interfacial deposition and transfer of TE is an SDS concentration below the CMC.

It is worth stressing that we have determined for the first time that bulk micellar solubilisation of a surfactant (SDS) for a drug (TE), although in equilibrium, is less efficient than the interfacial solubilisation and co-adsorption below the CMC. The experimental procedure described herein can be used to systematically study the interfacial interactions of surfactants with a wide range of small molecules as these interactions are important in the production of detergents, cosmetics, foods, pesticides, and drugs. In addition, by

estimating the best solubiliser based on its chemical composition, this work can be useful in surfactant design. The approach can be used to complement related bulk studies on drug self-assembly in micellar systems in the future.

Molecular Dynamics Simulations

The five simulations of SDS monolayers performed in the present study, namely MD0.1o, MD0.1s, MD0.1s+TE, MD1.0s+TE and MD1.0s+TE+TE, were designed to emulate several of the different experimental systems, both below and above the CMC, reported in the current study. Therefore, in each of these simulated systems the number of TE molecules present in each SDS monolayer and the area per surfactant molecule were varied such that they were representative of those values obtained from analysis of the corresponding SNR data. The three monolayers below the CMC, namely MD0.1o, MD0.1s, MD0.1s+TE, allow the effect of TE when the SDS monolayer interacts with a saturated solution of TE and when excess TE is added to this system to be studied. The systems MD1.0s+TE and MD1.0s+TE+TE allows for the SDS/TE monolayer, which would be in equilibrium with TE-saturated micelles in the bulk phase, to be investigated and how it is effected when excess TE is added to the monolayer.

Structure of sodium dodecyl sulfate monolayers in the presence of testosterone enanthate

As the number of TE molecules present increases, *d*-tail increases although the values of *d*-head are unchanged (Table 3), suggesting that the TE interacts predominately with the SDS tails as opposed to the SDS head groups, a result in agreement with that

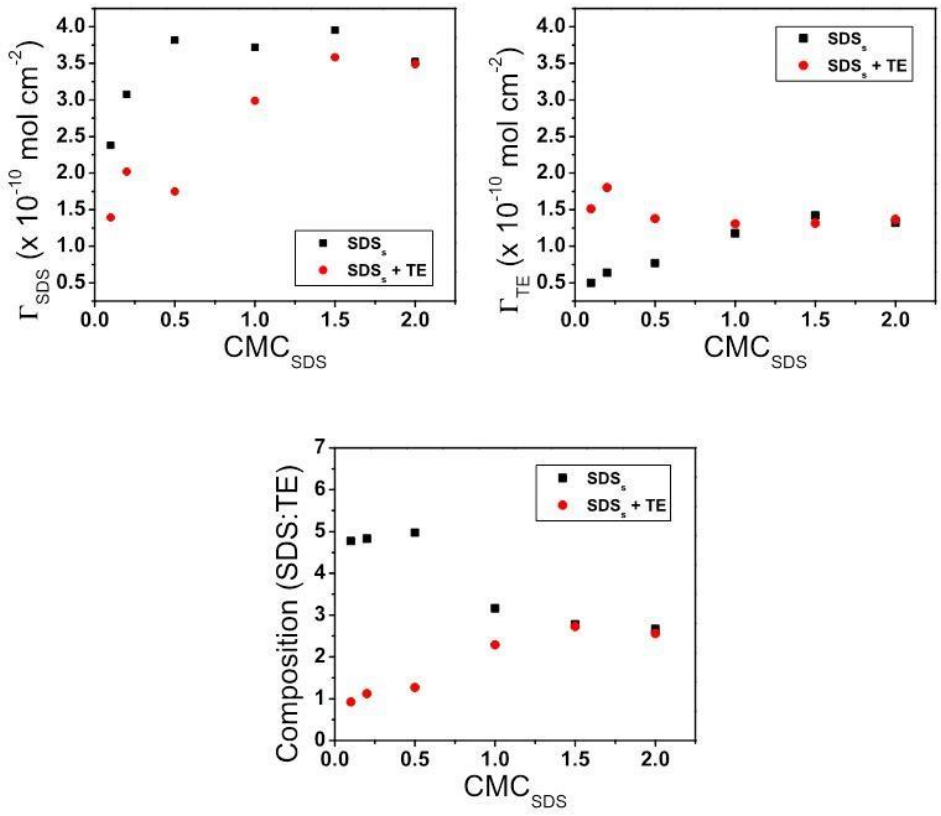

Figure 6: Surface excesses of SDS (top left), TE (top right) and interfacial composition (Γ_{SDS}/Γ_{TE}) of SDS/TE mixtures, as a function of SDS critical micelle concentration (CMC_{SDS}), before (SDSs) and after (SDSs+TE) spreading additional TE in a carrier solvent.

obtained from the SNR studies. Not surprisingly, when considering the large ratio of SDS to TE in the MD0.1s system, no change in the value of *d*-tail was observed between MD0.1o and MD0.1s, while in contrast a thicker *d*-tail region was seen when extra TE was added to the surface of the monolayer, again in agreement with the SNR results.

Figure 7 shows the probability distributions of ϑ_t for all the simulations. As anticipated, as the number of TE molecules in a monolayer increases, the mobility of the SDS tails decreases because the area per molecule in the x-y plane is reduced, which shifts the distribution in ϑ_t towards smaller angles. This observation is consistent with the trend of increasing *d*-tail with an increase in the relative proportion of TE in the SDS monolayer (Table 4) and from the SNR studies. As would be expected, there was no change in ϑ_t between MD0.1o and MD0.1s when there is very little TE in the monolayer while in contrast a larger change in ϑ_t was seen between MD0.1o/MD0.1s and MD0.1s+TE where one third of the molecules in the monolayer were TE. In the MD0.1s+TE system, the interaction of the SDS chains with the prevalent TE molecules causes them to become slightly more vertical than the MD0.1o/MD0.1s systems in which the SDS molecules adapt a configuration such that the hydrocarbons are oriented at their preferred angle at the air-water interface.

Figure 7 shows that the presence of the TE, regardless of the amount, results in a shift of the distribution of θ_h towards smaller angles. This result is the effect of the decrease in the area per molecule in the monolayers in the presence of TE. In addition, the distribution of head group angles becomes narrower as the SDS head groups preferentially orient themselves towards the aqueous medium and the reduction of area per molecule in the monolayer restricts the fluctuation in this angle.

The measured tilt angles of the SDS tails in MD0.1o are consistent with those that have been previously reported in other simulation studies of SDS at the air-water interface. Shi *et al.* found that the tilt angle of SDS tails decreases significantly as the area per molecule decreases,[44] and the values that they reported for monolayers with a range of areas per molecule that encompass those studied here agree well with those that we report. Pang *et al.* found that the tilt angle of SDS molecules of ~45 degrees for a monolayer in which the surfactants have an area per molecule of 50 Å^2.[45] This result is smaller than the tilt angle reported in this study, but this would be expected as the area per molecule in MD0.1o is larger.

Intrinsic density profiles of sodium dodecyl sulfate monolayers in the presence of testosterone enanthate

Intrinsic density profiles were calculated for all the monolayer simulations using a resolution of 0.5 Å (Figure 8). For all the simulations, a peak in water density is observed at *z* = 3.5 Å, which indicates that there is a layer of interfacial water in the head group region of the SDS monolayer with an increased density of water when compared to the bulk water.

Table 4: Average monolayer structural properties determined for all simulations conducted.

Property	MD0.1o	MD0.1s	MD0.1s+TE	MD1.0s+TE	MD1.0s+TE+TE
Composition (SDS:TE)	N/A	90:1	2:1	2.4:1	1.2:1
Area per SDS (Å^2)	78	78	159	48	48
θ_t (°)	55.0 ± 20.5	54.9 ± 20.6	49.0 ± 19.6	24.2 ± 13.9	26.0 ± 20.0
θ_h (°)	49.4 ± 24.0	48.5± 23.8	46.7 ± 23.0	34.9 ± 19.4	32.3 ± 18.7
d_{tail} (Å)	6.0 ± 0.2	6.1 ± 0.2	7.1 ± 0.3	10.8 ± 0.1	11.4 ± 0.3
d_{head} (Å)	2.2 ± 0.01	2.2 ± 0.01	2.2 ± 0.01	2.2 ± 0.01	2.2 ± 0.01
Roughness (Å)	2.4 ± 0.2	2.4 ± 0.2	2.3 ± 0.2	2.5 ± 0.2	4.9 ± 0.5
Surfactant hydration	8.3 ± 3.6	8.6 ± 3.8	5.5 ± 4.5	7.4 ± 3.5	7.6 ± 3.5
n_{H2O}	0.12	0.12	0.10	0.05	0.04

All errors are standard deviations

Figure 7: Angle distributions for the monolayer simulations. The top plot shows the surfactant, SDS chain tilt angle and the bottom shows the head group tilt angle, with or without TE.

The number density of oxygen atoms in water molecules converges to 0.033 at larger values of *z* which is equal to the target bulk density of 1 g/mL. For all the SDS and TE-containing SDS monolayer simulations, the number density of oxygen atoms in the water molecules decays into the monolayer hydrocarbon tail region. The magnitude of the number density of the oxygens in water molecules within the monolayer decreases as the relative number

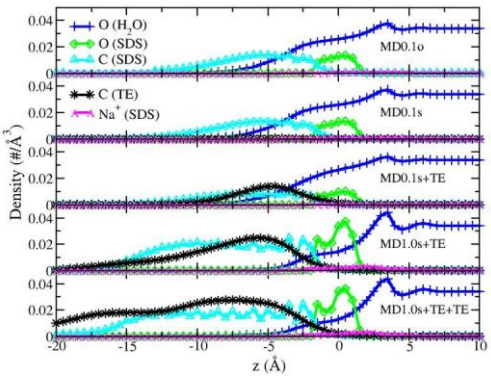

Figure 8: Intrinsic density plots for the TE monolayer simulations. The colours green, cyan and magenta are used to depict the density of SDS elements: oxygen, carbon, and sodium counterions respectively. The colours blue and black are used to depict the density of oxygen atoms in water and carbon atoms in TE molecules respectively.

of TE molecules present increases. This is a result of the simulations being carried with constant volume and therefore constant area for the monolayer and therefore as the amount of TE is increased the surfactant molecules are pressed closer to each other which results in the ejection of water into the bulk. To quantify this effect, the intrinsic density of water oxygen atoms was integrated over *z* from -□ to 0. This provides the average number of water molecules per unit area present within the monolayer hydrocarbon tail region, a quantity which will be referred to as n_{H2O} for the remainder of the manuscript. These values are displayed in Table 4 and show that n_{H2O} does indeed decrease as the relative number of TE molecules increases, for example for the MD0.1s+TE (0.10) and MD1.0s+TE (0.05) systems. Conversely, water penetration into the hydrocarbon tail region increases with the area per surfactant molecule. This is shown from the increase of n_{H2O} from ~0.04 to ~0.1 when the area per surfactant increases from 48 Å^2 to 70 Å^2, respectively. Moreover, the magnitude of the interfacial water peaks are larger for the systems above the CMC, namely MD1.0s+TE and MD1.0s+TE+TE than those below the CMC, namely MD0.1o, MD0.1s and MD0.1s+TE, indicating that there is a stronger localisation of water at the SDS/water interface for monolayers with a smaller area per surfactant molecule.

The sodium counter ions exhibit a single broad density peak with a relatively low density in comparison with the other components around the monolayer interface (-5 Å < *z* < 5 Å) in all systems, suggesting that they are situated near the interfacial region, which is also confirmed from visual inspection of the simulation trajectories. For clarity, density plots where the density scale has been enhanced to more clearly observe the density of the sodium counter ions have been included in the Supplementary Information, Figure SI5.

The intrinsic density profiles of carbon atoms in TE show that the drug is located amid the SDS hydrocarbon tails and not at the interface. As more TE molecules are added, the peak shifts slightly to smaller values of *z* but the magnitude of this peak is essentially unchanged. The density of TE molecules in the hydrocarbon tail and vacuum regions increases however. This suggests that as the preferred site of TE residence in the monolayer becomes saturated any additional TE molecules that are added to the monolayer are expelled from the monolayer to the vacuum region where they lie on the terminal carbons of the hydrocarbon tails rather than into the bulk water, which can be seen visually in Figure 9. Note that the density distributions observed in Figure 8 for the MD0.1o system are consistent with those of the head group and hydrocarbon tails observed in other simulation studies of SDS monolayers at the air-water interface.[44,45]

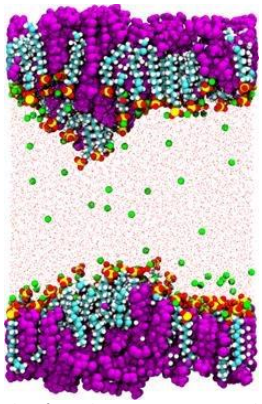

Figure 9: A snapshot from the MD1.0s+TE+TE production simulation illustrating the roughness induced by the excess TE molecules and where they are positioned as they are expelled to vacuum interface of the monolayer not into the aqueous sub-phase. The colours cyan, white, red, yellow and green are used to represent the elements: carbon, hydrogen, oxygen, sulfur and sodium respectively. The TE molecules are depicted in purple to distinguish them from the surfactants.

Orientation and position of testosterone enanthate in sodium dodecyl sulfate monolayers

The intrinsic density plots reveal that the TE molecules are generally situated within the SDS hydrocarbon tail region, however the plots do not contain any information about the orientation of TE at different positions within the monolayer, nor do they provide any specific detail about where the TE molecules are in reference to the surfactant molecules. Intrinsic drug angle distributions (Figure 10) were therefore constructed to provide insight into the range of orientations available to TE molecules at different positions within the SDS monolayers.

Figure 10 shows the distribution of the TE orientation as a function of distance from the intrinsic surface obtained from the monolayer simulations. For the MD0.1s system, the TE molecules

sample a wide range of orientations as shown by the broad probability distributions of cos(ϑ), however the distributions reveal that the preferred position and orientation of TE in this system is oriented in the *x-y* plane (probability peak at cos(ϑ) ~ 0) and resides in the largely in the C1-4 region, as shown by the prominent green curve in Figure 10. The TE molecules in the MD0.1s+TE simulation also adapt a similar orientation as those in MD0.1s, however the peak the in the distribution is shifted to slightly more negative values of cos(ϑ) ~ 0, showing that the TE molecules seemingly orient themselves such that their O1 atoms are slightly closer to the air-water interface than their O2 and O3 atoms. One way in which the distributions for MD0.1s+TE differ from those in MD0.1s is that there is a larger probability of finding TE in the head group region than in MD0.1s as indicated by the red curve, which is probably due to the larger amount of free space at the air-water interface due to the significantly larger area per molecule in this system.

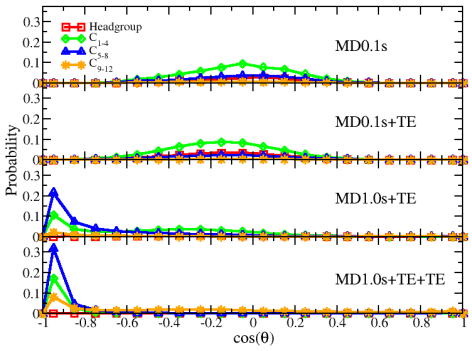

Figure 10: Intrinsic TE angle distributions for the different SDS monolayer simulations. The monolayer system is labelled in each subplot. For all plots, the colour scheme is consistent with the diagram in Figure 3(b) in that red, green, blue and orange are used to represent a TE molecule situated in the SDS head group, C1-4, C5-8 and C9-12 regions of the SDS monolayers respectively. Also note that in each subplot, the probability curves are normalised such that the sum of the area under the curves is equal to 1.

For the MD1.0s+TE and MD1.0s+TE+TE simulations, there is much more significant population of TE in the C5-8 region of the monolayer and the cos(ϑ) distributions in this region shift towards almost parallel drug orientation relative to the *z*-axis with the O1 atoms nearest the water interface due to packing constraints, as indicated by the sharp peak in the blue curves at cos(ϑ) ~ -0.95 (Figure 10). In the C1-4 region, the most prominent probability peak is also found at cos(ϑ) ~ -0.95, which means that the drugs in this region are also oriented parallel to the *z*-axis with O1 nearest the water when the surfactants are found in a smaller area per molecule configuration. In the MD1.0s+TE system, where there is less drug there are still some drug molecules in the C1-4 region oriented such that they are perpendicular to the z-axis, where as in MD1.0s+TE+TE there is no significant probability of find TE molecules with this orientation in the C1-4 region. Therefore, apparently, the TE molecules located within the C1-4 region orient themselves such that all the TE oxygen atoms are in contact with water within the monolayer and are thus able to maximise the number of hydrogen bonds between the water and these oxygen atoms in the TE molecules when there are not steric hindrances that would interfere with this orientation. When the systems become more densely packed (because of decreased area per molecule of the surfactant and/or more TE molecules), then the TE orients such that the O1 atoms are in contact with water and the end which contains the O2/O3 and the hydrocarbon chain moves away from the water interface and into the same region as the hydrocarbon tails of the surfactant molecules. As a result, the O2/O3 atoms become dehydrated, as the water molecules cannot penetrate very deeply into the SDS monolayer and are less able to do so as more TE is added.

In the MD1.0s+TE+TE simulation, there is a significant proportion of the TE molecules found in the C9-12 region of the monolayer of surfactants. This highlights the fact that at such high concentrations of drug molecules, the drug prefers to lie on top of the monolayer rather than be forced into the aqueous sub-phase of the system. It should be noted that while the majority of the TE molecules in the C9-12 region of the monolayer are still oriented such that they are parallel to the *z*-axis with the O1 atom closest to the water interface, there is a small population of the drug molecules that are oriented such that they are lying perpendicular to the *z*-axis, which are also those drug molecules lying on top of the monolayer of SDS (as can be seen in Figure 9).

Interfacial hydration of the sodium dodecyl sulfate monolayers in the presence of testosterone enanthate

The histograms of the average hydration number for each monolayer simulation exhibited unimodal distributions (see the Supplementary Information, Figure SI6). The probability distributions do not change drastically when the number of TE molecules per monolayer is varied, however the mean hydration number does decrease slightly as the number of TE molecules per monolayer is increased, except for the case of MD1.0s+TE+TE which has a larger mean hydration number than MD1.0s+TE. This observation is attributed to the increased monolayer roughness which results in an increase of the surface area of surfactant head groups exposed to the solvent (as can be seen also in Figure 9). The mean hydration numbers for all the simulations are stated in Table 4.

Conclusions

The apparent aqueous solubility of poorly water soluble drugs can be improved by solubilisation within surfactant micelles. Recent work suggests that the location of a drug in the micelle may influence its stability, loading capacity, release rate and consequently therapeutic effect. Information on the preferred site of drug solubilisation within a particular micelle is lacking. We describe an experimental protocol which, for the first time, has

been performed to systematically study the interfacial structure and composition of monolayers containing a model low-dose, poorly water soluble drug (TE) and a surfactant (SDS). Interfacial properties were used as an experimentally accessible model platform to link to the bulk properties given the presence of dynamic equilibrium between interfacial processes and bulk aggregation behavior. To understand the equilibrium conditions of SDS/TE mixtures at the air-water interface, results obtained from ST and SNR experiments have been explored further with MD simulations.

Fitting models obtained from specular neutron reflectivity data suggest adsorption of TE in the C_{12} hydrophobic tail region for SDS concentrations both above and below the CMC prior to, and after the additional spreading of TE at the interface. No significant change in the monolayer structure, even after the spreading of additional TE at the interface was observed for the micellar SDS solutions. An increase in head group hydration and area per molecule was observed after the spreading of additional TE at SDS concentrations below the CMC. These observations are confirmed by MD simulations. Also in agreement with MD simulations is the monolayer thickness obtained from SNR.

The stoichiometry of SDS:TE at the air-water interface at SDS concentrations above the CMC was determined to be approximately the same as the 3:1 obtained from bulk solubilisation studies, and remained the same after the additional spreading of TE at the interface. Until now, the solubilisation capacity of surfactant micelles for poorly water-soluble chemicals has not been estimated explicitly from interfacial properties. Interestingly the stoichiometry of SDS:TE changed from 5:1 to 1:1 after the additional spreading of TE at the interface, possibly suggesting that SDS concentrations below the CMC are better interfacial solubilisers of TE.

Questions about the equilibrium of the system emerged for the SDS/TE monolayers at SDS concentrations below the CMC as spreading of additional TE on the monolayer caused a pronounced reduction in surface tension. Even so, ST results revealed the achievement of equilibrium conditions in the SDS/TE mixtures above the CMC because of consistency in surface tension prior to and after the additional spreading of TE. Information on the SDS/TE mixtures above the CMC reflects maximum solubilisation of TE in the bulk despite the geometric differences between micelles and interfaces. This interpretation was confirmed by the results of constant composition of SDS/TE for micellar SDS solutions even after the additional spreading of TE at the interface.

MD simulations reveal that when TE is present in SDS monolayers at low concentrations, the drug lies in a perpendicular orientation to the C_{12} hydrophobic tail. As the drug concentration is increased within a fixed monolayer area, the drugs tend to insert deeper into the hydrophobic region of the monolayer, where they tend to adopt a more parallel orientation with respect to the surfactant tails with their more polar end containing the O1 atom nearest the air-water interface. The surfactants in the monolayers become more ordered with the addition of drug molecules, as confirmed by the decrease in the mean surfactant chain tilt angles. Additionally, in the MD simulations, it was observed that once the SDS monolayer is saturated with TE molecules, any excess TE molecules will remain at the vacuum/monolayer interface as opposed to being transferred into the aqueous sub-phase.

Investigation of hydrogen bonding between water molecules in the monolayer simulations revealed that the number of hydrogen bonds formed between neighbouring water molecules decreases as the monolayer is approached, and this is because of the reorientation of water molecules interacting with the electric field due to the negatively charged SDS head groups.

We have gained important insights on the adsorption properties of SDS/TE mixtures at the air-water interface using ST, SNR and MD simulations. Our findings have shown that bulk solubilisation of TE in SDS micelles are consistent with and therefore may be inferred from the interfacial results obtained in the present study. Our approach can be extended in the future to explore the interactions of other hydrophobic molecules such as perfumes, pesticides and polymers at the air-water interface, and this information should ideally be supported by complementary information from bulk micellisation studies. Consequently, the present study is a basis for further studies for understanding other surfactant-based systems at the air-water interface and paves the way for the design of new surfactants with enhanced drug solubilisation capacity. Indeed studies are underway to understand the relationship between the location of TE and related drugs in planar SDS monolayers and in the corresponding micelles to determine the effect of the packing of the aliphatic chains of the surfactant into the curved micelles on the extent and preferred site of solubilisation of drug.

Formatted: Font color: Auto

Conflicts of Interest

There are no conflicts of interest to declare.

Acknowledgements

The authors acknowledge GETFund for funding of the Ph.D. of Y. S., the ILL for allocations of beam time on FIGARO (DOIs: 10.5291/ILL-DATA.9-10-1348 and 10.5291/ILL-DATA.9-10-1435), Simon Wood for technical assistance and Andrea Tummino for help in the data analysis. D. T. A. and C. D. L. thank the EPSRC for the studentship which funds D. T. A.'s research. Additionally, D. T. A. and C. D. L. acknowledge the stimulating research environment provided by the EPSRC Centre for Doctoral Training in Cross-Disciplinary Approaches to Non-Equilibrium Systems (CANES, EP/L015854/1). Finally, it is through C.D.L.'s membership within the UK HPC Materials Chemistry Consortium, which is funded by the Office of Science and Technology through the EPSRC High End Computing Programme (Grant No. EP/L000202), that we could use the facilities of ARCHER, the UK National Supercomputing

Service (http://www.archer.ac.uk), to carry out the molecular dynamics simulations used in of this work.

Notes and references

1. Babu, N. J.; Nangia, A. Crystal Growth and Design 2011, 11, 2662–2679.
2. Tong, W.-Q.; Wen, H. In Water-Soluble Formulation; Liu, R, Ed.; CRC Press, Taylor and Francis: Boca Raton, Fl. 2008; p. 63.
3. Thayer, A. M. Chem. Eng. News 2010, 88, 13–18.
4. Lu, J. R,; Li, Z. X.; Thomas, R. K.; Binks, B. P.; Crichton, D.; Flecther, P. D. I.; McNab, J. R. J. Phys. Chem. B 1998, 102, 5785–5793.
5. Lu, J. R.; Su, T. U.; Lawrence, M. J.; Barlow, D. J.; Warisnoicharoen, W.; Zuberi, T. J. Phys. Chem. B 1999, 103, 4638–4658.
6. Bradbury, R.; Penfold, J.; Thomas, R. K.; Tucker, I. M.; Petkov, J. T.; Jones, C. Langmuir 2013, 29, 3361–3369.
7. Brabury, R.; Penfold, J.; Thomas, R. K.; Petkov, J. T. J. Coll. Interfac. Sci. 2016, 461, 352–358.
8. Yan, H.; Cui, D.; Bu-Liu, C.; Yuan, S.-L. Langmuir 2011, 28, 4931–4938.
9. Schwarze, M.; Volovych, L.; Wille S.; Mokrushina, L.; Arlt, W.; Schmöcacker, R. Ind. Eng. Chem. Res. 2012, 51, 1846–1852.
10. Storm, S.; Jakobtorweihen, S.; Smirnova, I.; Panagiotopoulos, A. Z. Langmuir 2013, 29, 11582–11592.
11. Allen, D. T.; Saaka, Y.; Lawrence, M. J.; Lorenz, C. D. J. Phys. Chem. B 2014, 118, 13192–13201.
12. Liang, X.; Marchi, M.; Guo, C.; Dang, Z.; Abel, S. Langmuir 2016, 32, 3645–3654.
13. Xing, H.; Yan, P.; Xiao, J.-X. Soft Matter 2013, 9, 1164–1171.
14. Soleimanzadegan, S.; Farsi, H.; Ebrahimi, F. J. Molec. Struct. 2015, 1079, 494–501.
15. Ferreira, J. V. N.; Capello, T. M.; Siqueira, L. J. A.; Lago, J. H. G.; Caseli, L. Langmuir 2016, 32, 3234–3241.
16. Griffith, E. C.; Perkins, R. J.; Telesford, D.-M.; Adams, E. M.;Cwiklik, L.; Allen, H. C.; Roeselova, M.; Vaida, V. J. Phys. Chem. B 2015, 119, 9038–9048.
17. Korchowiec, B.; Korchowiec, J.; Orlog-Naturalna, M.; Regnouf de Vains, J.-B.; Rogalska, E. Colloid Surf. B 2016, 145, 777–784.
18. Basak, U. K.; Datta, A.; Bhattacharyya, D. Colloid. Surf. B 2015, 132, 34–44.
19. Dabkowska, A. P.; Collins, L. E.; Barlow, D. J.; Barker, R.; McLain, S. E.; Lawrence, M. J.; Lorenz, C. D. Langmuir 2014, 30, 8803–8811.
20. Lorenz, C. D.; Hsieh, C.-M.; Dreiss, C. A.; Lawrence, M. J. Langmuir 2010, 27, 546–553.
21. Saaka, Y. Ph.D. Thesis, University of London, 2016.
22. Malcolmson, C. A. Ph.D. Thesis, University of London, 1992.
23. Malcolmson, C.; Satra, C.; Kantaria, S.; Sidhu, A.; Lawrence, M. J. J. Pharm. Sci. 1998, 87, 109116.
24. Lu, J. R.; Purcell, I. P.; Lee, E. M.; Simister, E. A.; Thomas, R. K.; Rennie, A. R.; Penfold, J. J. Colloid Interfac. Sci. 1995, 174, 441–455.
25. Vargaftik, N. B.; Volkov, B. N.; Voljak, L. D. J. Phys. Chem. Ref. Data 1983, 12, 817–820.
26. Campbell, R. A.; Wacklin, H. P.; Sutton, I.; Cubitt, R.; Fragneto, G. Eur. Phys. J. Plus 2011, 126, 107.
27. Lu, J. R.; Thomas, R. K.; Penfold, J. Adv. Colloid Interfac. Sci. 2000, 84, 143–304.
28. Braun, L.; Uhlig, M.; von Klitzing, R.; Campbell, R. A. Adv. Colloid Interfac. Sci. 2017, 247, 130–148.
29. Nelson, A. J. Appl. Cryst. 2006, 39, 273–276.
30. Durchschlag, H.; Zipper, P. In Ultracentrifugation; Lechner, M. D.,Ed.; Progress in Colloid & Polymer Science; Steinkopff, 1994; pp 20–39.
31. Braslau, A.; Deutsch, M.; Pershan, P. S.; Weiss, A. H.; Als-Nielsen, J.; Bohr, J. Phys. Rev. Lett. 1985, 54, 114–117.
32. Campbell, R. A.; Tummino, A.; Noskov, B. A.; Varga, I. Soft Matter 2016, 12, 5304–5312.
33. Martinez, L.; Andrade, R.; Birgin, E. G.; Martinez, J. M. J. Comput. Chem. 2009, 30, 2157–2164.
34. Plimpton, S. J. Comput. Phys. 1995, 117, 1–19.
35. Vanommeslaeghe, K.; Hatcher, E.; Acharya, C.; Kundu, S.; Zhong, S.; Shim, J.; Darian, E.; Guvench, O.; Lopes, P.; Vorobyov, I.; Mackerell, A. J. Comput. Chem. 2010, 31, 671–690.
36. Yu, W.; He, X.; Vanommeslaeghe, K.; MacKerell, A. D. J. Comput. Chem. 2012, 33, 2451–2468.
37. Klauda, J. B.; Venable, R. M.; Freites, J. A.; OConnor, J. W.; Tobias, D. J.; Mondragon-Ramirez, C.; Vorobyov, I.; Alexander D.; MacKerell, J.; Pastor, R. W. J. Phys. Chem. B 2010, 114, 7830–7843.
38. Pastor, R. W.; MacKerell Jr., A. D. J. Phys. Chem. Lett. 2011, 2, 1526–1532.
39. Jorgensen, W. L.; Chandrasekhar, J.; Madura, J. D.; Impey, R. W.; Klein, M. L. J. Chem. Phys. 1983, 79, 926–935.
40. Darden, T.; York, D.; Pedersen, L. J. Chem. Phys. 1993, 98, 10089–10092.
41. Hoover, W. G. Phys. Rev. A 1985, 31, 1695–1697.
42. Ryckaert, J.-P.; Ciccotti, G.; Berendsen, H. J. J Comp. Phys. 1977, 23, 327–341.
43. Pandit, S. A.; Bostick, D.; Berkowitz, M. L. J. Chem. Phys 2003, 119, 2199–2205.
44. Shi, L.; Tummala, N. R.; Striolo, A. Langmuir 2010, 26, 5462–5474.
45. Pang, S.; Wang, Y.; Xu, G.; Han, T. J. Phys. Chem. B 2011, 115, 2518–2526.